

# Conversion of Methanol to Hydrocarbons over Phosphorus-modified ZSM-5/ZSM-11 Intergrowth Zeolites

Peng Li · Weiping Zhang · Xiuwen Han ·  
Xinhe Bao

Received: 19 August 2009 / Accepted: 2 November 2009 / Published online: 13 November 2009  
© Springer Science+Business Media, LLC 2009

**Abstract** The phosphorus-modified ZSM-5/ZSM-11 intergrowth zeolites has been used for the catalytic conversion of methanol to hydrocarbons. As evidenced by MAS NMR and NH<sub>3</sub>-TPD, the modification by phosphorus leads a distinct decrease of the Brønsted acid sites and the acid strength of the catalysts in comparison with the parent ZSM-5/ZSM-11, which causes a dramatic improvement of the selectivity towards propylene. At 400 °C, the ratio of propylene to ethylene can reach about 8.0. A comparison with the conventional ZSM-5 zeolite has been also carried out in the present study.

**Keywords** Methanol to hydrocarbons · ZSM-5/ZSM-11 · Intergrowth zeolites · Phosphorus modification · Propylene

## 1 Introduction

Ethylene and propylene are very important petrochemical products. To meet the growing demand for olefins, methanol to olefins (MTO) and methanol to propylene (MTP) processes are promising in the future [1]. Olefin selectivity is a key issue for methanol conversion. With the propylene

demand growing quickly in recent years, much more attention has been paid to methanol or DME to propylene reaction recently. High selectivity of propylene has been obtained on modified ZSM-5 zeolites [2, 3]. Phosphorus-modified ZSM-5 has been extensively investigated in methanol conversion [4–14], and catalytic cracking reaction [15–20]. The structure of p-modified ZSM-5 has been characterized by many research groups [21–27]. Phosphorus modification is an effective method in MTO and MTP reactions. Introduction of Phosphorus into ZSM-5 can enhance light olefin selectivity while significantly reducing aromatic selectivity.

MFI has a straight channel and sinusoidal channel intersecting with each other. MEL is formed by two sets of straight channels. The pore dimension between MFI and MEL is almost the same and the formation of intergrowth zeolitic structure is possible. The structure of ZSM-5/ZSM-11 intergrowth zeolites has been characterized by HREM [28–32], X-ray diffraction [33] and Fluorescence Microscopy [34, 35]. The structure segment of ZSM-5/ZSM-11 is made up of inversion center of MFI and mirror symmetry of MEL connecting with pentasil chains. ZSM-5/ZSM-11 intergrowth zeolites have been used in catalytic reactions, such as n-decane cracking reaction [36] and benzene alkylation with dilute ethylene to ethylbenzene [37, 38]. It exhibits intermediate catalytic performance between MFI and MEL structure in n-decane cracking reaction. ZSM-5/ZSM-11 has been considered an excellent catalyst in converting benzene with dilute ethylene in FCC (fluid catalytic cracking) off-gas to ethylbenzene reaction. However, there is little report of ZSM-5/ZSM-11 intergrowth zeolites in the methanol conversion reaction. In this study, the p-modified ZSM-5/ZSM-11 intergrowth zeolites were prepared and characterized by various techniques and evaluated in the methanol to hydrocarbons (MTH) reaction.

**Electronic supplementary material** The online version of this article (doi:10.1007/s10562-009-0214-6) contains supplementary material, which is available to authorized users.

P. Li · W. Zhang (✉) · X. Han · X. Bao (✉)  
State Key Laboratory of Catalysis, Dalian Institute of Chemical Physics, Chinese Academy of Sciences, 457 Zhongshan Road, 116023 Dalian, China  
e-mail: wpzhang@dicp.ac.cn

X. Bao  
e-mail: xhbao@dicp.ac.cn

As a comparison, the commonly used ZSM-5 zeolite has also been modified and tested in the MTH reaction.  $^1\text{H}$  MAS NMR and  $\text{NH}_3$ -TPD have been applied to detect the acidity of the catalysts. The variations of the acidity after post-treatment via phosphorus modification may be correlated to the catalytic performance in MTH reaction.

## 2 Experimental

### 2.1 Catalyst Preparation

HZSM-5 zeolite was purchased from Nan Kai Company, China. HZSM-5/ZSM-11 intergrowth zeolites were provided by BASF Chemical Company, Germany. They are commercial products and used as received. The p-modified zeolite samples were prepared by impregnating 1.0 g catalyst into 10 mL aqueous solution containing desired amount of phosphoric acid. The suspension was dried at 50 °C for 24 h under vacuum, and finally calcined at 550 °C for 3 h. P-modified zeolites containing  $\times$  wt% of phosphorus were denoted as xP-ZSM-5 and xP-ZSM-5/ZSM-11.

### 2.2 Catalyst Characterization

#### 2.2.1 XRD, $\text{N}_2$ Adsorption

XRD patterns were obtained at room temperature on a Rigaku D/Max-RB diffractometer using  $\text{CuK}\alpha$  radiation. Powder patterns of the samples were recorded over a range of  $2\theta$  values from 5 to 50° at 40 kV and 100 mA with a scanning rate of 5 deg/min. The integrated signal intensities at  $2\theta = 23.2, 23.8, 24.3^\circ$  were used to calculate the relative crystallinity [39].

Nitrogen adsorption experiments were performed at  $-196$  °C on an ASAP 2000 system in the static measurement mode. Samples were degassed at 350 °C for 10 h before the measurements. Specific surface areas were calculated by the Multipoint BET method, and the total pore volume was determined by  $\text{N}_2$  adsorption at a relative pressure of 0.99.

#### 2.2.2 MAS NMR Measurements

All NMR spectra were recorded on a Varian Infinityplus-400 spectrometer.  $^{27}\text{Al}$  MAS NMR spectra were recorded at a resonance frequency of 104.2 MHz with a spinning rate of 10 kHz. Chemical shifts were referenced to  $(\text{NH}_4)\text{Al}(\text{SO}_4)_2 \cdot 12\text{H}_2\text{O}$  at  $-0.4$  ppm as a secondary reference. The spectra were accumulated for 1,024 scans with  $\pi/4$  pulse width of 1.8  $\mu\text{s}$  and 2 s recycle delay.  $^{29}\text{Si}$  MAS NMR spectra were obtained at 79.4 MHz using 7.5-mm MAS probe with a spinning rate of 4 kHz. Chemical shifts were referenced to 4,4-dimethyl-4-silapentane sulfonate

sodium (DSS). 1,024 scans were accumulated with a  $\pi/4$  pulse width of 2.15  $\mu\text{s}$  and a 4 s recycle delay.  $^{31}\text{P}$  MAS NMR spectra were measured with proton high power decoupling, and  $\text{H}_3\text{PO}_4$  as chemical shift reference at a resonance frequency of 161 MHz.  $^{31}\text{P}$  MAS NMR was recorded using 4 s recycle delay,  $\pi/4$  pulse width of 1.5  $\mu\text{s}$ . Before the  $^1\text{H}$  MAS NMR measurements, samples were dehydrated at 450 °C over 20 h under the pressure below  $10^{-2}$  Pa.  $^1\text{H}$  MAS NMR spectra were collected at 399.9 MHz with a 4 s recycle delay, 80 scans and spinning rate of 10 kHz. Chemical shifts were referenced to adamantane. The Dmfit software was used to deconvolution using fitted Gaussian–Lorentzian line shapes [40].

#### 2.2.3 $\text{NH}_3$ -TPD

Temperature-Programmed Desorption of Ammonia ( $\text{NH}_3$ -TPD) measurements were carried out in a conventional U-shaped stainless-steel micro-reactor (i.d. = 4 mm) using flowing helium (He) as the carrier gas. The  $\text{NH}_3$ -TPD process was monitored by an on-line gas chromatograph (Shimadzu GC-8A) equipped with a TCD detector. Typically 0.14 g sample was pretreated at 600 °C for 1 h in flowing He (25 mL/min), then cooled to 150 °C and saturated with  $\text{NH}_3$  gas. After that, the sample was purged with pure He stream for certain time until a stable GC-baseline was attained. Finally  $\text{NH}_3$ -TPD experiment was carried out in the range of 150–600 °C at a heating rate of 18.8 °C/min.

### 2.3 Catalytic Evaluation

Methanol conversion was carried out under atmosphere pressure in a continuous reacting system with quartz fixed-bed reactor loading 60 mg powder catalyst. Methanol was fed to reactor from a saturator using  $\text{N}_2$  carrier gas. The saturator temperature was kept at 26.1 °C (methanol  $\text{WHSV} = 2 \text{ h}^{-1}$ ) by a thermostatic bath. Before each catalytic test, the catalyst was activated in situ for 1 h at 450 °C under  $\text{N}_2$  flow to remove the moisture and cooled down to the desired temperatures. The gas sample was injected into GC after 10 min at each temperature, and then the system was switched to  $\text{N}_2$  flow and heated to the next temperature point. The product distribution was analyzed by on-line gas chromatography (HP 6890) equipped with a flame ionization detector and 30-m HP-PLOT Q capillary column.

## 3 Results and Discussion

### 3.1 XRD Patterns and $\text{N}_2$ Adsorption Data

XRD patterns of ZSM-5 and ZSM-5/ZSM-11 intergrowth zeolites are shown in Fig. 1. The parent ZSM-5 and

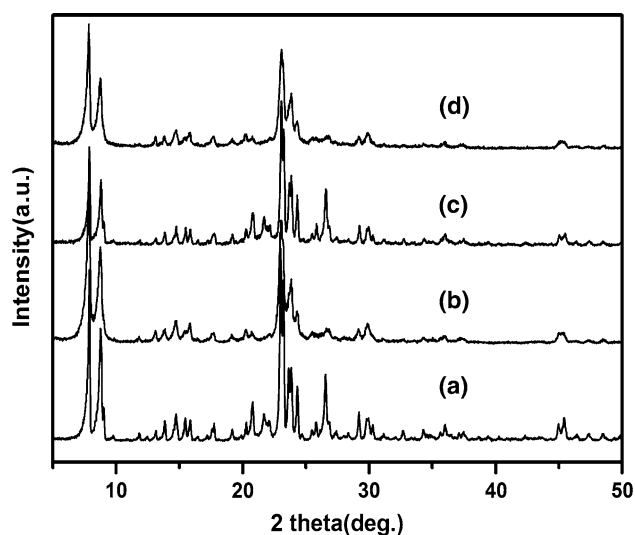


**Fig. 1** XRD patterns of **a** HZSM-5; **b** HZSM-5/ZSM-11; **c** 4P-ZSM-5; **d** 4P-ZSM-5/ZSM-11

intergrowth ZSM-5/ZSM-11 zeolites show high crystallinity. ZSM-5 has the typical MFI structure. The XRD pattern at  $2\theta = 20\text{--}25^\circ$  has three peaks in ZSM-5 sample and two obvious peaks at  $2\theta = 44\text{--}48^\circ$ . ZSM-11 has two peaks at  $2\theta = 20\text{--}25^\circ$  and only one peak at  $2\theta = 44\text{--}48^\circ$  according to the literature [41]. These are the main differences between ZSM-5 and ZSM-11 from the XRD profiles. By comparing the pattern features in Fig. 1a and b, it is clear that there is MEL phase in ZSM-5/ZSM-11 intergrowth zeolites besides the MFI phase. But we can not tell the exact amount of each phase from XRD patterns because of the peak overlapping. The relative crystallinities of p-modified samples in Table 1 indicate obvious decrease, which may be due to the serious dealumination as can be seen from the following MAS NMR measurements. The BET surface area and pore volume of ZSM samples calculated by  $\text{N}_2$  adsorption are listed in Table 1. The total pore volume of ZSM-5/ZSM-11 is larger than that of ZSM-5 probably due to additional volume in cavity formed at the intersections of the channels and/or interparticle voids [29].

**Table 1** BET surface areas, silicon to aluminum ratios, relative crystallinities and pore volumes of the catalysts

Sample	Si/Al <sup>a</sup>	$S_{\text{BET}}$ ( $\text{m}^2/\text{g}$ )	Relative crystallinity <sup>b</sup>	Total pore volume ( $\text{cm}^3/\text{g}$ )
HZSM-5	26	367	100	0.22
HZSM-5/ZSM-11	25	392	100	0.36
4P-ZSM-5	55	192	68	0.15
4P-ZSM-5/ZSM-11	103	311	63	0.33

<sup>a</sup> Calculated from  $^{29}\text{Si}$  MAS NMR spectra

<sup>b</sup> Based on XRD patterns

Phosphorus modification results in a decrease in the surface area and pore volume, which may be also ascribed to dealumination caused by the phosphorus.

### 3.2 $^{27}\text{Al}$ MAS NMR

$^{27}\text{Al}$  MAS NMR spectra can be used to determine the coordination of the aluminum species in aluminasilicate zeolite. Figure 2 shows  $^{27}\text{Al}$  MAS NMR spectra of parent and p-modified samples. For H-form samples, a strong sharp peak can be observed at 54 ppm which can be assigned to tetrahedral framework aluminum species [39]. And a relatively weak signal can be seen at 0 ppm which can be attributed to octahedral aluminum species, indicating that there exists small amount of extra-framework aluminum in H-form catalyst (see Fig. 2a, b). When ZSM-5 and ZSM-5/ZSM-11 zeolites were impregnated with phosphorus acid, many new peaks appeared at ca.  $-14$  ppm and ca.  $30\text{--}40$  ppm. The former peak is due to octahedral aluminum attached to phosphorus atom [42]. And the assignment of latter peaks can be difficult because too broad peaks overlapping. It can be attributed to tetrahedral aluminum in a distorted environment at framework location [43]. Zhuang et al. [15] ascribed the broad resonance to the interaction of  $\text{H}_3\text{PO}_4$  with extra-framework aluminum that might lead to the formation of different types of aluminum phosphate. It exhibits as broad resonance in one dimensional  $^{27}\text{Al}$  MAS NMR. In contrast to 4P-ZSM-5, much more framework aluminum has been removed over 4P-ZSM-5/ZSM-11 intergrowth zeolites from  $^{27}\text{Al}$  MAS NMR spectra. This may be due the better chemical stability of ZSM-5 than ZSM-11 upon acid treatment according to the results of Simon et al. [44]. In our case dealumination occurs more easily over ZSM-5/ZSM-11 intergrowth zeolites.

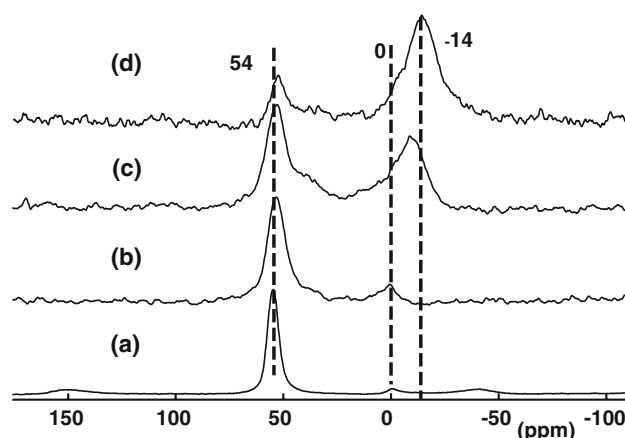


**Fig. 2**  $^{27}\text{Al}$  MAS NMR spectra of **a** HZSM-5; **b** HZSM-5/ZSM-11; **c** 4P-ZSM-5; **d** 4P-ZSM-5/ZSM-11

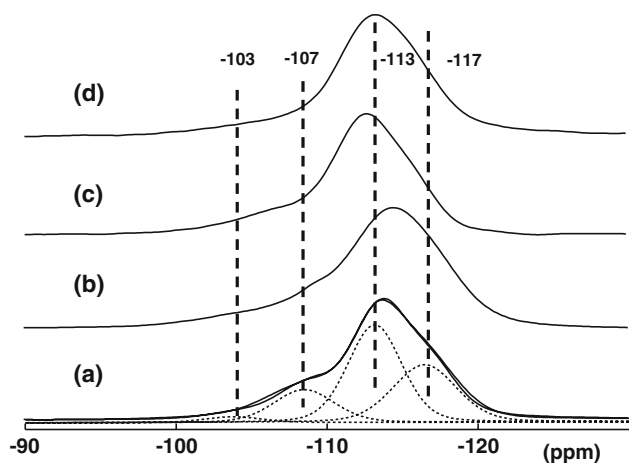


**Fig. 3**  $^{29}\text{Si}$  MAS NMR spectra of **a** HZSM-5; **b** HZSM-5/ZSM-11; **c** 4P-ZSM-5; **d** 4P-ZSM-5/ZSM-11

### 3.3 $^{29}\text{Si}$ MAS NMR

Figure 3 shows  $^{29}\text{Si}$  MAS NMR spectra of the p-modified zeolite samples. The resonances at  $-113$  and  $-117$  ppm are attributed to the crystallographically inequivalent sites of the  $\text{Si}(\text{OSi})_4$  groups in ZSM-5 and ZSM-5/ZSM-11 zeolites [39]. The peak at  $-107$  ppm is assigned to  $\text{Si}(\text{OAl})(\text{OSi})_3$  groups. The peak at  $-103$  ppm is ascribed to the silanols with the structure of  $\text{Si}(\text{OSi})_3\text{OH}$ . According to the Loewenstein's rule, the framework Si/Al ratios of the zeolites can be calculated by deconvolution of the  $^{29}\text{Si}$  MAS NMR spectra. As shown in Table 1, the framework Si/Al ratio increased obviously because of dealumination occurring during phosphorus modification procedure. It can be seen that the framework Si/Al increased much higher over ZSM-5/ZSM-11 intergrowth zeolites than that of ZSM-5. This is consistent with the results from  $^{27}\text{Al}$  MAS NMR.

### 3.4 $^{31}\text{P}$ MAS NMR

Figure 4 presents  $^{31}\text{P}$  MAS NMR spectra of p-modified ZSM-5 and ZSM-5/ZSM-11 intergrowth zeolites. The

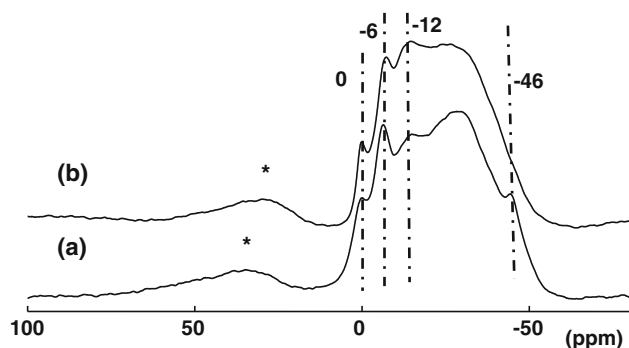


**Fig. 4**  $^{31}\text{P}$  MAS NMR spectra of **a** 4P-ZSM-5; **b** 4P-ZSM-5/ZSM-11, \* denotes spin sideband

resonance at ca. 0 ppm is ascribed to excess phosphorus species which did not interact with framework aluminum [21, 24, 25]. The signal at ca.  $-6$  ppm is associated with phosphorus species in pyrophosphorus or polyphosphoric acid [25, 26, 45, 46]. The peak at ca.  $-12$  ppm is assigned to p species for middle groups of pyrophosphorus or other short-chain polyphosphates [46]. The lines at  $-20$  to  $-40$  ppm are very broad. The assignments of these peaks are still controversial. According to the literature, these signals can be attributed to aluminum phosphate or highly condensed polyphosphate species. The resonance at  $-46$  ppm is due to P species in  $\text{P}_4\text{O}_{10}$  [26, 47, 48]. It can be seen that P species on ZSM-5 and ZSM-5/ZSM-11 are almost the same except that p-modified ZSM-5 has much more  $\text{P}_4\text{O}_{10}$ . This is because dealumination occurs severely over ZSM-5/ZSM-11 compared to ZSM-5, and a lot of phosphorus acid may not react with framework aluminum on ZSM-5 zeolite. After the zeolite was calcined, many P species exist as  $\text{P}_4\text{O}_{10}$  remaining on ZSM-5.

### 3.5 $^1\text{H}$ MAS NMR

High-resolution  $^1\text{H}$  MAS NMR is a powerful and direct approach for characterizing the acidic sites in zeolites.  $^1\text{H}$  MAS NMR spectra of p-modified ZSM-5 and ZSM-5/ZSM-11 zeolites are presented in Fig. 5. The signals between  $-0.5$  and  $0.5$  ppm is attributed to the non-acidic unperturbed extra-framework aluminum hydroxyls [49]. The low-field peak at ca. 2.4 ppm is nonframework Al-OH due to hydrogen bond between Al-OH and neighbouring oxygen atoms. The silanol groups appear at 1.8 ppm. The bridging hydroxyl groups, namely Brønsted acid site can be observed at 3.9 ppm [50]. The main peak in Fig. 5a is at 3.9 ppm indicating a lot of Brønsted acid sites in parent ZSM-5. Compared to ZSM-5, the amount of silanol groups is higher than that of Brønsted acid sites on ZSM-5/ZSM-11

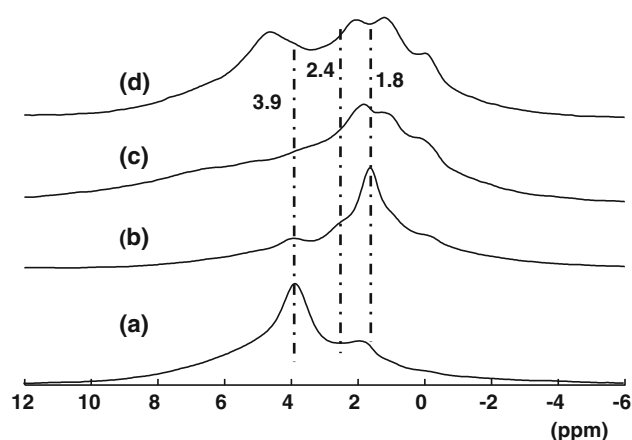


**Fig. 5**  $^1\text{H}$  MAS NMR spectra of **a** HZSM-5; **b** HZSM-5/ZSM-11; **c** 4P-ZSM-5; **d** 4P-ZSM-5/ZSM-11

11(see Fig. 5b). The intensity at 3.9 ppm decreases obviously after phosphorus impregnation due to extraction of aluminum from the zeolitic framework and the subsequent appearance of phosphorus species at about 5.0 ppm. These have been proven by  $^{27}\text{Al}$  MAS NMR and  $^{29}\text{Si}$  MAS NMR spectra.

### 3.6 $\text{NH}_3$ -TPD

Figure 6 shows the  $\text{NH}_3$ -TPD profiles of all the samples. For the parent HZSM-5, there are two peaks in the spectrum. The first one is at 265 °C, which is attributed to weak acid site. The second peak is at 470 °C, which is ascribed to strong acid site. Compared to HZSM-5, the desorption of HZSM-5/ZSM-11 is almost the same peak location while the intensity is much lower due to the lower amount of Brønsted acid sites. The temperature of desorption peaks over p-modified samples reveal the different acid strength (see Fig. 6c, d). It can be seen that high temperature peak almost disappears in 4P-ZSM-5/ZSM-11 sample. And the low temperature peak shifts from 265 to 292 °C, indicating that p-modified ZSM-5/ZSM-11 increases weak acid strength. Similar phenomenon happened on 4P-ZSM-5. But the strong acid sites show a broad peak at about 400 °C on 4P-ZSM-5. It means that acid strength remained in 4P-ZSM-5 is much higher than that remained in 4P-ZSM-5/ZSM-11.

### 3.7 Catalytic Performance of P-Modified ZSM-5 and ZSM-5/ZSM-11 Intergrowth Zeolites for Methanol to Hydrocarbons Reaction

The catalytic performances of p-modified ZSM zeolites for MTH reaction in the temperature range of 250–550 °C are shown in Fig. 7. The temperature effect on methanol

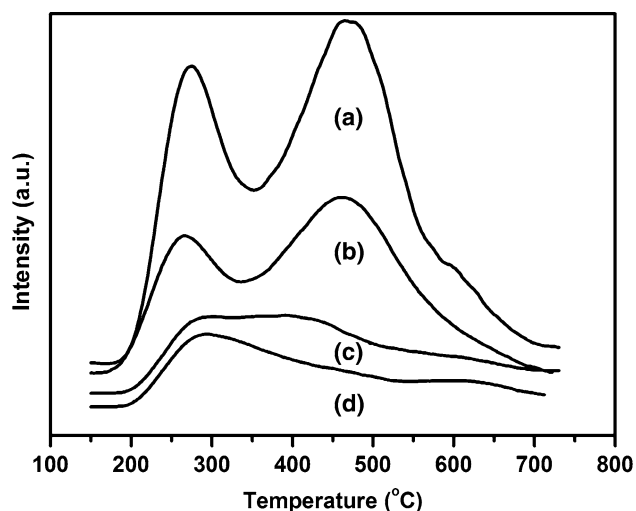


**Fig. 6**  $\text{NH}_3$ -TPD profiles of **a** HZSM-5; **b** HZSM-5/ZSM-11; **c** 4P-ZSM-5; **d** 4P-ZSM-5/ZSM-11

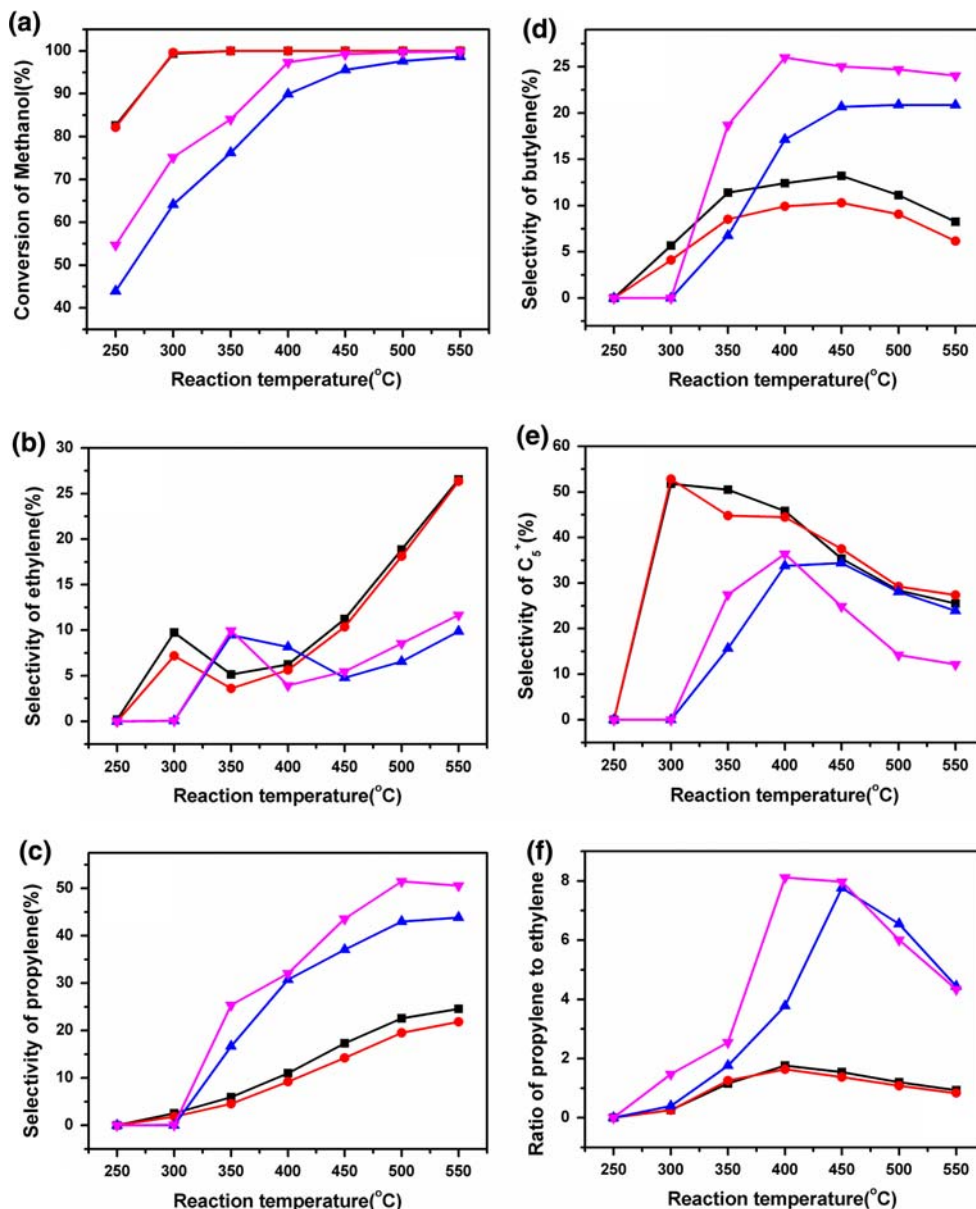
conversion is similar between HZSM-5 and HZSM-5/ZSM-11 intergrowth zeolites, it reaches 100% above 300 °C(see Fig. 7a). The p-modified sample exhibits different catalytic behavior in methanol conversion. The methanol conversion increased with temperature increasing over p-modified samples. The need for high temperature for methanol conversion may be due to the decrease in acid strength and Brønsted acid amount on p-modified zeolites as indicated by above  $\text{NH}_3$ -TPD and  $^1\text{H}$  MAS NMR results.

The general trend for ethylene selectivity increases with increasing temperatures on the parent zeolites. The p-modified sample shows lower ethylene selectivity below 10% compared to the parent samples at higher temperatures (Fig. 7b). The selectivity of propylene also increases with increasing temperatures (Fig. 7c). Propylene selectivity can be improved obviously on p-modified samples. The acid strength decrease of p-modified sample is responsible for the propylene selectivity improvement. One reason is that phosphorus modification can suppress hydrogen transfer reaction. The acid strength is relevant to hydrogen transfer reaction [51]. Another reason was proposed that propylene oligomerization were suppressed on the p-modified catalyst because the formation of bulky phosphorus compounds block the sterically demanding reactions [13].

$\text{C}_4^-$  selectivity follows the same trend as propylene selectivity. The p-modified ZSM-5/ZSM-11 shows the highest  $\text{C}_4^-$  selectivity of about 25% at 400 °C (Fig. 7d). It should be noted that after phosphorus modification, the selectivity of ethylene decreased compared to parent ZSM sample in contrast to the selectivities of propylene and butylene increasing. BjØrgen et al. [52–55] proposed two cycles of light olefins production on ZSM-5 zeolite. One route is ethylene and aromatics cycle and another one is  $\text{C}_3^+$  alkenes cycle. Ethylene may be formed from lower methylbenzenes. Propylene and higher alkenes may be formed from alkenes methylation and cracking reactions. Our above results show that the trend of ethylene selectivity is different from that of propylene and butylene, which, to some extent, also supports BjØrgen's proposal. It was possible to tune zeolite acidity via post-modification to make  $\text{C}_3^+$  alkenes formation dominant in product distribution. The different acid strength between p-modified ZSM-5 and ZSM-5/ZSM-11 may result in the enhancement of propylene and butylene selectivity.

When the selectivity of light olefin increases, obviously the selectivity of  $\text{C}_5^+$  decreases correspondingly on p-modified samples (Fig. 7e). Phosphorus modification suppresses the secondary reaction and reduced the amount of aromatics and alkanes [4]. So, p-modified ZSM-5/ZSM-11 has lower  $\text{C}_5^+$  selectivity than that on ZSM-5 at higher temperatures.

**Fig. 7** Catalytic performances of p-modified ZSM-5 and ZSM-5/ZSM-11 intergrowth zeolites in MTH reaction. Methanol conversion (a); selectivities of ethylene (b); propylene (c); butylenes (d); C<sub>5</sub>+ (e); Ratio of propylene to ethylene (f). ZSM-5 (black square); ZSM-5/ZSM-11 (red circle); 4P-ZSM-5 (blue triangle); 4P-ZSM-5/ZSM-11 (pink inverted triangle)



The ratio of propylene to ethylene can reach about 8.0 over 4P-ZSM-5/ZSM-11, which is almost twice than that on 4P-ZSM-5 at 400 °C (Fig. 7f). Phosphorus modification can distinctly enhance selectivity of light olefins and propylene over ZSM-5/ZSM-11 intergrowth zeolites.

DME as a product was calculated in the catalyst selectivity. DME selectivity decreased to zero over parent samples above 300 °C (see Supplement Fig. S1a). The DME over p-modified samples can completely convert to hydrocarbons above 400 °C. DME selectivity is almost the same between parent ZSM-5 and ZSM-5/ZSM-11. The selectivity of olefins (C<sub>2</sub>–C<sub>4</sub>) is above 80% at 500 °C over 4P-ZSM-5/ZSM-11 zeolites. 4P-ZSM-5/ZSM-11 zeolites exhibit higher selectivity of light olefins than 4P-ZSM-5 (Supplement Fig. S1b). P-modified ZSM zeolites exhibit

much lower alkanes selectivity (Supplement Fig. S1c) because secondary reaction, such as hydrogen transfer reaction can be suppressed due to acid strength reduction [56].

#### 4 Conclusions

It is found that p-modified ZSM-5/ZSM-11 intergrowth zeolites show better catalytic performance in MTH reaction than ZSM-5. The selectivities of propylene and olefins are improved obviously compared to ZSM-5. The propylene to ethylene ratio reaches about 8.0 at 400 °C over p-modified ZSM-5/ZSM-11 intergrowth zeolites. Characterizations suggest that the acid strength plays an important role in

increasing light olefin selectivity. The reduction of acid strength can improve the selectivity of propylene and butylene and decrease the selectivity of ethylene and aromatics over ZSM-5/ZSM-11 intergrowth zeolites. p-modified ZSM-5/ZSM-11 intergrowth zeolites may become a potential catalyst for methanol conversion to propylene.

**Acknowledgments** We thank Dr. Ulrich Müller and Dr. Bilge Yilmaz of BASF Chemical Company, Germany for providing the ZSM-5/ZSM-11 intergrowth zeolites. We also thank Dr. X. J. Li. of DICP for help with the NH<sub>3</sub>-TPD measurements. We are grateful for the financial support of the National Natural Science Foundation of China and the Ministry of Science and Technology of China through the National Key Project of Fundamental Research (No. 2009CB623507).

## References

1. Stocker M (1999) *Microporous Mesoporous Mater* 29:3–48
2. Zhao TS, Takemoto T, Yoneyama Y, Tsubaki N (2005) *Chem Lett* 34:970–971
3. Zhao TS, Takemoto T, Tsubaki N (2006) *Catal Commun* 7:647–650
4. Kaeding WW, Butter SA (1980) *J Catal* 61:155–164
5. Védrine JC, Auroux A, Dejaifve P, Ducarme V, Hoser H, Zhou S (1982) *J Catal* 73:147–160
6. Rahman A, Lemay G, Adnot A, Kaliaguine S (1988) *J Catal* 112:453–463
7. Suzuki K, Kiyozumi Y, Matsuzaki K, Ikai S, Shin S (1988) *Appl Catal* 39:315–324
8. Ikai S, Okamoto M, Nishioka H, Miyamoto T, Matsuzaki K, Suzuki K, Kiyozumi Y, Sano T, Shin S (1989) *Appl Catal* 49:143–163
9. Rahman A, Adnot A, Lemay G, Kaliaguine S, Jean G (1989) *Appl Catal* 50:131–147
10. Dehertog WJH, Froment GF (1991) *Appl Catal* 71:153–165
11. Tynjala P, Pakkanen TT, Mustamaki S (1998) *J Phys Chem B* 102:5280–5286
12. Tynjala P, Pakkanen TT (1998) *Microporous Mesoporous Mater* 20:363–369
13. Abubakar SM, Marcus DM, Lee JC, Ehresmann JO, Chen CY, Kletnieks PW, Guenther DR, Hayman MJ, Pavlova M, Nicholas JB, Haw JF (2006) *Langmuir* 22:4846–4852
14. Kaarsholm M, Joensen F, Nerlov J, Cenni R, Chaouki J, Patience GS (2007) *Chem Eng Sci* 62:5527–5532
15. Zhuang JQ, Ding M, Gang Y, Yan ZM, Liu XM, Liu XC, Han XW, Bao XH, Peng X, Liu ZM (2004) *J Catal* 228:234–242
16. Zhao GL, Teng JW, Xie ZK, Jin WQ, Yang WM, Chen QL, Tang Y (2007) *J Catal* 248:29–37
17. Blasco T, Corma A, Martinez-Triguero J (2006) *J Catal* 237:267–277
18. Xue NH, Chen XK, Nie L, Guo XF, Ding WP, Chen Y, Gu M, Xie ZK (2007) *J Catal* 248:20–28
19. Jiang G, Zhang L, Zhao Z, Zhou X, Duan A, Xu C, Gao J (2008) *Appl Catal A Gen* 340:176–182
20. Xue NH, Nie L, Fang DM, Guo XF, Shen JY, Ding WP, Chen Y (2009) *Appl Catal A Gen* 352:87–94
21. Damodaran K, Wiench JW, de Menezes SMC, Lam YL, Trebosc J, Amoureux JP, Pruski M (2006) *Microporous Mesoporous Mater* 95:296–305
22. Lercher JA, Rumplmayr G (1986) *Appl Catal* 25:215–222
23. Jentys A, Rumplmayr G, Lercher JA (1989) *Appl Catal* 53:299–312
24. Seo G, Ryoo R (1990) *J Catal* 124:224–230
25. Caro J, Bülow M, Derewinski M, Haber J, Hunger M, Kärger J, Pfeifer H, Storek W, Zibrowius B (1990) *J Catal* 124:367–375
26. Lischke G, Eckelt R, Jerschke HG, Parltitz B, Schreier E, Storek W, Zibrowius B, Öhlmann G (1991) *J Catal* 132:229–243
27. de Menezes SMC, Lam YL, Damodaran K, Pruski M (2006) *Microporous Mesoporous Mater* 95:286–295
28. Thomas JM, Millward GR (1982) *J Chem Soc Chem Commun* 1380–1383
29. Millward GR, Ramdas S, Thomas JM, Barlow MT (1983) *J Chem Soc Faraday Trans 2* 79:1075–1082
30. Terasaki O, Thomas JM, Millward GR, Watanabe D (1989) *Chem Mater* 1:158–162
31. Hay DG, Jaeger H, Wilshier KG (1990) *Zeolites* 10:571–576
32. Ohsuna T, Terasaki O, Nakagawa Y, Zones SI, Hiraga K (1997) *J Phys Chem B* 101:9881–9885
33. Jablonski GA, Sand LB, Gard JA (1986) *Zeolites* 6:396–402
34. Karwacki L, Stavitski E, Kox MHF, Kornatowski J, Weckhuysen BM (2007) *Angew Chem Int Ed* 46:7228–7231
35. Roeflaers MJB, Ameloot R, Baruah M, Uji-i H, Bulut M, De Cremer G, Muller U, Jacobs PA, Hofkens J, Sels BF, De Vos DE (2008) *J Am Chem Soc* 130:5763–5772
36. Francesconi MS, Lopez ZE, Uzcategui D, Gonzalez G, Hernandez JC, Uzcategui A, Loaiza A, Imbert FE (2005) *Catal Today* 107–08:809–815
37. Xu L, Liu J, Wang Q, Liu S, Xin W, Xu Y (2004) *Appl Catal A* 258:47–53
38. Song Y, Liu S, Wang Q, Xu L, Zhai Y (2006) *Fuel Process Technol* 87:297–302
39. Zhang W, Bao X, Guo X, Wang X (1999) *Catal Lett* 60:89–94
40. Fayon F, Massiot D, Capron M, King I, Le Calvé S, Alonso B, Durand J-O, Bujoli B, Gan Z, Hoatson G (2002) *Magn Reson Chem* 40:70–76
41. Kokotailo GT, Chu P, Lawton SL, Meier WM (1978) *Nature* 275:119–120
42. Caeiro G, Magnoux P, Lopes JM, Ribeiro ER, Menezes SMC, Costa AF, Cerqueira HS (2006) *Appl Catal A Gen* 314:160–171
43. Yan Z, Ma D, Zhuang J, Liu X, Liu X, Han X, Bao X, Chang F, Xu L, Liu Z, Mol J (2003) *Catal A Chem* 194:153–167
44. Simon MW, Nam SS, Xu WQ, Suib SL, Edwards JC, Oyoung CL (1992) *J Phys Chem* 96:6381
45. Grimmer AR, Haubenreisser U (1983) *Chem Phys Lett* 99:487–490
46. Duncan TM, Douglas DC (1984) *Chem Phys* 87:339–349
47. Müller D, Jahn E, Ladwig G, Haubenreisser U (1984) *Chem Phys Lett* 109:332–336
48. Blackwell CS, Patton RL (1984) *J Phys Chem* 88:6135–6139
49. Hunger M, Ernst S, Steuernagel S, Weitkamp J (1996) *Microporous Mater* 6:349–353
50. Hunger M (1997) *Catal Rev Sci Eng* 39:345–393
51. Yuen L-T, Zones SI, Harris TV, Gallegos EJ, Auroux A (1994) *Microporous Mater* 2:105–117
52. Svelle S, Joensen F, Nerlov J, Olsbye U, Lillerud K-P, Kolboe S, Bjørgen M (2006) *J Am Chem Soc* 128:14770–14771
53. Bjørgen M, Svelle S, Joensen F, Nerlov J, Kolboe S, Bonino F, Palumbo L, Bordiga S, Olsbye U (2007) *J Catal* 249:195–207
54. Svelle S, Olsbye U, Joensen F, Bjørgen M (2007) *J Phys Chem C* 111:17981–17984
55. Bjørgen M, Joensen F, Lillerud K-P, Olsbye U, Svelle S (2009) *Catal Today* 142:90–97
56. Haw JF, Song WG, Marcus DM, Nicholas JB (2003) *Acc Chem Res* 36:317–326